

Magnetorotons in moiré fractional Chern insulators

Xiaoyang Shen,^{1,*} Chonghao Wang,^{1,*} Xiaodong Hu,^{2,*} Ruiping Guo,^{1,3}
Hong Yao,³ Chong Wang,^{1,†} Wenhui Duan,^{1,3,4,5,‡} and Yong Xu^{1,4,6,§}

¹State Key Laboratory of Low Dimensional Quantum Physics and
Department of Physics, Tsinghua University, Beijing, 100084, China

²Department of Material Science and Engineering,
University of Washington, Seattle, WA 98195, USA

³Institute for Advanced Study, Tsinghua University, Beijing 100084, China

⁴Frontier Science Center for Quantum Information, Beijing, China

⁵Beijing Academy of Quantum Information Sciences, Beijing 100193, China

⁶RIKEN Center for Emergent Matter Science (CEMS), Wako, Saitama 351-0198, Japan

(Dated: February 24, 2025)

The discovery of fractional Chern insulators (FCIs) unlocks exciting opportunities to explore emergent physical excitations arising from topological and geometric effects in novel phases of quantum matter. Here we investigate the intraband neutral excitations, namely magnetorotons, in moiré FCIs within twisted MoTe₂ by applying the Girvin, MacDonald, and Platzman (GMP) ansatz together with the method of dynamical geometric response. We reveal the universal existence of the finite-momentum magnetorotons in moiré FCIs and predict their characteristic scales. Furthermore, we explore the geometric nature of magnetorotons in the long-wavelength limit, identifying their gapped chiral nature with angular momentum-2, which originates from the momentum-space incompressibility of FCIs. Utilizing the excellent tunability of moiré systems, we extend our analysis to other incompressible phases and uncover the dynamical properties of geometric excitations influenced by quantum phase transitions. Finally, we provide experimental proposals for detecting and advancing the study of intraband neutral excitations in moiré FCIs.

Introduction.— Recent experimental discovery of fractional Chern insulators (FCIs) in twisted transition metal dichalcogenide (TMD) homobilayers has sparked intensive interest in exploring novel quantum states in moiré systems [1–8]. FCIs can be regarded as the zero-field, lattice analog of fractional quantum Hall (FQH) states, henceforth inheriting the intrinsic topological nature of the FQH phase and the potential for quantum computation [9, 10]. Numerous theoretical studies [11–18] have predicted the existence of FCIs in moiré materials, which are likely to give rise to emergent physics beyond the conventional lowest Landau level (LLL) framework [19–27]. While most research focused on studying the ground state properties of FCIs, the low-lying collective excitations that could encode the significant information related to the topological and geometric properties of FCIs remain largely unexplored [28–30].

A celebrated hallmark of FQH states is the existence of intraband neutral excitations, known as *magnetorotons*, proposed by Girvin, MacDonald, and Platzman (GMP) [31]. Such kind of neutral excitations can be effectively described using a density wave ansatz within the framework of the single mode approximation (SMA), which reveals a “roton-like” local minimum at finite momentum. The GMP theory further demonstrates that in the long-wavelength limit, the energy dispersion of magnetorotons is gapped and can be interpreted as biexcitons with quadrupole structure due to the $(q\ell_B)^4$ behavior of cross section [32–35]. Recent studies [36–41] have revealed that magnetorotons of FQH in the long-wavelength limit can be interpreted as excitations of the

internal quantum metric. These excitations exhibit a chiral spin-two nature, earning the name of “massive chiral gravitons” [42–47]. The remarkable features of geometric excitations have been experimentally observed a few months ago [48–50]. The study of magnetorotons in FQH systems naturally motivates the exploration of similar excitations in FCIs hosted in moiré flatbands. The exceptional tunability of moiré systems facilitates the study of magnetorotons not only in ideal FCIs but also in less ideal FCIs undergoing transitions to competing phases, offering opportunities to uncover intriguing physics beyond the conventional LLL framework.

In this Letter, we provide a comprehensive study of the magnetorotons in FCIs hosted by the twisted MoTe₂. We evaluate the magnetoroton dispersion by generalizing the GMP ansatz to FCIs, and find the universal existence of magnetorotons at finite momentum. We then analyze the dynamical geometric response of magnetorotons in the long-wavelength limit. In ideal FCIs, the geometric excitations process definite chirality near the zero-momentum magnetoroton energy. Those geometric excitations originate from the momentum-space incompressibility of FCI fluid and can be interpreted as multipolar quantum fluctuations on the uniform charge density background in momentum space. The geometric excitations in FQH and FCI fluid can be unified into the incompressibility of the space-momentum phase space. We find new indicators of FCI stability from the perspective of excitations. We extend the analysis to the geometric excitations in other incompressible phases and find the Berry curvature and quantum metric play decisive roles

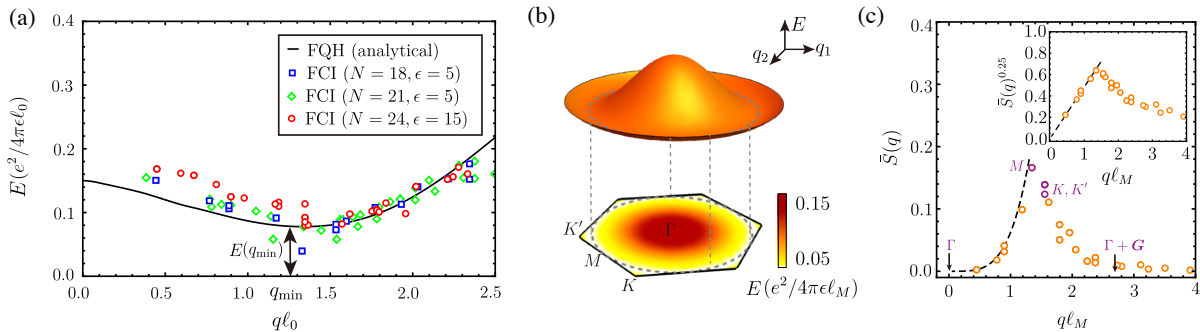


FIG. 1. (a) Energy dispersions of magnetorotons in FCIs obtained for different numbers of k-points (N) used in ED and varying dielectric constant ϵ . The black curve denotes the analytical results deduced from the GMP algebra for disk FQH. ℓ_0 represents ℓ_B in FQH and ℓ_M in FCIs. (b) Three-dimensional diagram illustrating the magnetoroton dispersion. The local minimum resides close to the M points. (c) The projected structure factor $\bar{S}(\mathbf{q})$ at $N = 18, \epsilon = 5$. $\bar{S}(\mathbf{q})$ scales as $(q\ell_M)^4$ in the long-wavelength limit. High symmetry points are labeled in the figure. The inset is the linear fitting of $\bar{S}^{0.25}(q)$ versus q .

in the diverse behaviors of excitations. Finally, we give proposals for detecting these intraband neutral excitations, providing a pathway for experimental exploration.

Model.— Recent experiments [1–8] have observed prominent signatures of FCI in twisted homobilayer MoTe₂ around a twisted angle $\theta \sim 4^\circ$ and a fractional filling $\nu = -\frac{2}{3}$, with an estimated dielectric constant $\epsilon \sim 5 - 15$. We start with the continuum model of twisted bilayer MoTe₂ [51] using the aforementioned parameters: $\mathcal{H} = \mathcal{H}_0 + V$. Here \mathcal{H}_0 is the single particle moiré Hamiltonian as described in Sec. I of the Supplemental Material (SM). V is the Coulomb interaction $V = \frac{1}{2A} \sum_{\mathbf{q}} V(\mathbf{q}) : \hat{\rho}(\mathbf{q}) \hat{\rho}(-\mathbf{q}) :$. A denotes the area of the two-dimensional system, \mathbf{q} is the momentum, $V(\mathbf{q}) = \frac{2\pi \tanh(qd)}{\epsilon\epsilon_0 q}$ is the dual-gate screened Coulomb interaction, d is the gate-to-sample distance, and “:” means normal ordering. $\hat{\rho}(\mathbf{q}) = \sum_{\mathbf{k}} \Lambda_{\mathbf{k}, \mathbf{q}} \hat{c}_{\mathbf{k}+\mathbf{q}}^\dagger \hat{c}_{\mathbf{k}}$ is the density operator projected into the highest valence band that hosts the FCI state, where $\Lambda_{\mathbf{k}, \mathbf{q}} = \langle u_{\mathbf{k}+\mathbf{q}} | u_{\mathbf{k}} \rangle$ is the form factor and $|u_{\mathbf{k}}\rangle$ is the periodic part of Bloch eigenstates of \mathcal{H}_0 , and $\hat{c}_{\mathbf{k}}^\dagger$ is the corresponding creation operator. Starting from this continuum model, previous studies [11–18] have revealed that the topmost valence band is an ideally flat band with non-trivial Chern number $\mathcal{C} = 1$, demonstrating the emergence of FCI phases. We provide the detailed band structure and the exact diagonalization (ED) spectrum based on the continuum model, and further verify the existence of an FCI as its ground state (see Sec. I of the SM).

Magnetorotons in ideal moiré FCIs.— To investigate the magnetorotons in FCI, the GMP ansatz in FQH with the SMA [31] is used, and a density-wave-like excitation of FCIs is assumed as $|\psi_{\mathbf{q}}\rangle = \hat{\rho}(\mathbf{q})|\psi_0\rangle$, $|\psi_0\rangle$ is the many-body ground state from the ED, and $\hat{\rho}(\mathbf{q})$ is the projected density operator. The GMP ansatz is able to properly describe the low-lying intraband neutral excitations in

FCI on the following aspects: (i) $|\psi_{\mathbf{q}}\rangle$ is orthogonal to ground state $|\psi_0\rangle$ when $\mathbf{q} \neq 0$ and thus is truly an excited state. (ii) The density operator projected to the topmost valence band characterizes the low energy intraband excitons. (iii) The ansatz is build from the ground state of FCI, inheriting the topological and geometric nature of the FCI. The variational expectation energy of $|\psi_{\mathbf{q}}\rangle$ is $E_{\mathbf{q}} = \frac{\langle \psi_{\mathbf{q}} | H | \psi_{\mathbf{q}} \rangle}{\langle \psi_{\mathbf{q}} | \psi_{\mathbf{q}} \rangle} - E_0$, where the ground state energy E_0 is chosen as the energy reference.

The energy dispersions of magnetorotons in FCIs calculated by using different numbers N of k points and varying dielectric constant ϵ are shown in Fig. 1(b). After rescaling, we observe that the dispersions are full-range gapped and there exists a universal local minimum of the dispersion at a mediate value of momentum $q_{\min} \sim 1.3/\ell_M$, $\ell_M \equiv \sqrt{\sqrt{3}/4\pi a_M} \sim 2\text{nm}$ ($a_M \approx a_0/\theta$ is the length of a moiré unit cell) is the characteristic length analogous to the magnetic length ℓ_B ($\ell_B = \sqrt{\hbar/eB} \sim 20\text{nm}$) in FQH. This matches with the unclosed GMP-like algebra at the long-wavelength limit in FCI, $[\hat{\rho}(\mathbf{q}), \hat{\rho}(\mathbf{q}')] \approx i\Omega \mathbf{q} \times \mathbf{q}' \hat{\rho}(\mathbf{q} + \mathbf{q}') + \mathcal{O}(q^3)$, $\Omega \approx 2\pi/S_{\text{BZ}} = \ell_M^2$ is the flatband Berry curvature and S_{BZ} is the area of 1st Brillouin zone (BZ). The minimum resides between the M point and the K point in the first BZ, showing a magnetoroton gap $E(q = q_{\min}) \sim 0.08e^2/(4\pi\epsilon\ell_M) \approx \Delta_{\text{mb}}$, where Δ_{mb} is the many-body gap or the energy of the first excited state in ED spectrum. At $q = q_{\min}$ the overlap between the GMP wavefunction and the exact first excitation state reaches 98.22% at $N = 18$, confirming the reliability of the GMP ansatz in studying FCIs. The extrapolation to zero-momentum gives a gap $E(q = 0) \sim 0.17e^2/(4\pi\epsilon\ell_M) \approx 2.125\Delta_{\text{mb}}$. The zero momentum gap remains robust for various parameters, interaction strengths, and finite-size effects. At small q , we also extract the projected static structure factor $\bar{S}(q) \equiv \langle \psi_{\mathbf{q}} | \psi_{\mathbf{q}} \rangle$. At the long wavelength

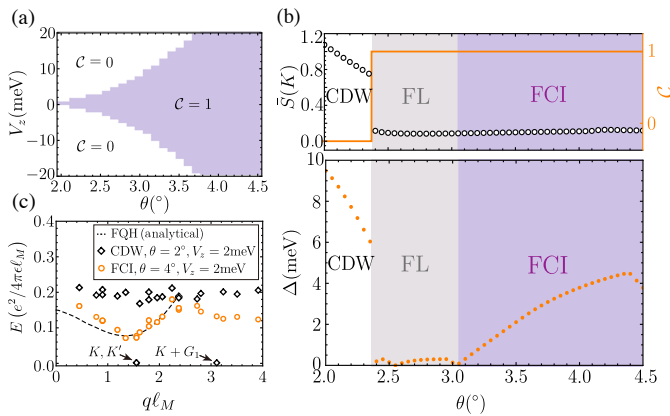


FIG. 2. (a) Topology of the topmost valence band in twisted MoTe₂ as a function of vertical displacement field V_z and twisted angle θ . (b) Phase structure indicators at small displacement field $V_z = 2\text{meV}$ as a function of twisted angle θ . In the upper panel of (b) the dots are the projected static structure factor $\bar{S}(q)$ at K points that exhibit a peak at CDW phases and are featureless at gapless and FCI phases. The orange line is the Chern number of the topmost valence band. In the bottom panel of (b) the solid orange dots are the many-body gap Δ computed by ED. (c) Variational energy from the SMA for $V_z = 2\text{meV}$ with $\theta = 2^\circ$ (FCI) and $\theta = 4^\circ$ (CDW). At the CDW phase, the magnetoroton is softened at commensurate momenta.

limit, the projected form factor $\bar{S}(q)$ vanishes as $(q\ell_M)^4$ at $q \rightarrow 0$ limit, indicating the intraband excitations at long-wavelength limit have the quadruple structure.

Magnetorotons in FCI-CDW transition.— Charge density wave (CDW) is one of FCI's major competitors in moiré systems [52–56]. In the twisted MoTe₂ system, a topological transition from $\mathcal{C} = 1$ to $\mathcal{C} = 0$ can be induced by either tuning the twisted angle θ or the vertical displacement field V_z , inducing the possibility of FCI-CDW phase transition [28, 57–65]. It is intriguing to investigate the GMP ansatz after FCI-CDW phase transition.

A typical phase transition induced by changing the twisted angle from 4° to 2° at a fixed displacement field $V_z = 2\text{meV}$ is shown in Fig. 2(d). At $\theta = 4^\circ$, the system is in the FCI phase hosted by a $\mathcal{C} = 1$ band, and the dispersion exhibits a local minimum at finite q . From $\theta = 4^\circ$ to $\theta = 2^\circ$, in the vicinity of gap closing, the spectrum is gapless and the ground state is Fermi liquid (FL). At $\theta = 2^\circ$, the system is in the $\mathcal{C} = 0$ CDW phase with a three-fold ground state $|0\rangle = |\psi_0\rangle, |\psi_K\rangle, |\psi_{K'}\rangle$, and the dispersion of magnetorotons is nearly flat and features a sizable gap, except at the commensurate momenta K and $K' + n\mathbf{G}$ where the neutral excitation energy is nearly zero. This means that in the CDW phase, the excitations become soft at those momenta, as expected from the fact that the static form factor $\bar{S}(q)$ exhibits peaks at those momenta and thus leads to small E_q . The overlap between the GMP wavefunction $\hat{\rho}(K)|\psi_0\rangle$ and the ED ground state $|\psi_K\rangle$ at K reaches 98.98%, indicating

that in CDW phase, the GMP ansatz $\hat{\rho}(K)|\psi_0\rangle = |\psi_K\rangle$ is the charge density wave with wavevector K .

Geometric excitations in FCIs and their proximate phases.— So far, the property of long-wavelength magnetorotons in FCI remains elusive. In the following, we demonstrate that the excitations come from the momentum-space incompressibility of the FCI fluid.

We start with the single-particle 4D phase space $x = (x_1, x_2, k_1, k_2)$ of a 2D system. The canonical transformation f preserving commutator $[x_i, k_j] = \delta_{ij}$, $i, j = 1, 2$ in general is expressed to be $f_i : x'_i \rightarrow x_i + \nabla_{k_i} h(x)$, $k'_i \rightarrow k_i - \nabla_{x_i} h(x)$, $i = 1, 2$, $h(x)$ is the differentiable function of x . Mapping f_i also preserves the volume element $dx_i \wedge dk_i$ according to Liouville's theorem.

In FQH, due to LLL band projection, the momentum is related to position via $k_z \rightarrow \bar{z}, k_{\bar{z}} \rightarrow z$. The 4D phase space is then projected to the 2D real space [66]. f thus keeps the volume element $dx_1 \wedge dk_1 \rightarrow dx_1 \wedge dx_2$ invariant, rendering real-space incompressibility. f forms a Lie group consisting volume-preserving diffeomorphism (VPD) in 2D, and the Lie algebra is the classical w_∞ algebra with generators $\hat{\mathcal{L}}_m^\ell \sim z^{m+1} \bar{z}^{\ell+1}$, $m, \ell \geq -1, [z, \bar{z}] = 1$. The generators generate the geometric excitations $\hat{\mathcal{L}}_m^\ell |0\rangle$ with higher angular momentum l , for example $l = 2$ mode generated by $\hat{\mathcal{L}}_1^{-1}, \hat{\mathcal{L}}_{-1}^1$ [39].

In ideal FCI with LLL-like flatband [67], via band projection 4D phase space is reduced to the 2D momentum space and recover the momentum-space volume-preserving symmetry. The geometric excitations from the momentum-space incompressibility of FCI then behave like multipolar charge distribution fluctuation $\hat{n}_{\mathbf{k}} - \langle \hat{n}_{\mathbf{k}} \rangle$ on the uniform background in the momentum space.

For the systems that are not residing on the LLL-like flatband, the band projection does not relate the momentum with the position, henceforth the phase space volume-preserving symmetry can not reduce to real (or momentum) space volume-preserving symmetry, rendering the breakdown of w_∞ algebra (or GMP algebra). Henceforth geometric excitations fundamentally come from the volume-preserving symmetry of enlarged phase space and can only be reduced to 2D subspace in LLL physics (See SM Sec. IV for details).

To investigate the energy of the excitations, we study the change of energy (band-projected Hamiltonian) after distortion f , $\hat{\mathcal{O}} := \delta_f H \approx \delta_f V$. Generally in a Bloch band, the Berry connection and quantum metric encoded in the band-projected interaction $V(A, g)$ are different from LLL-like flatband and fluctuate in k space, giving rise to distinct behaviors of geometric excitations in FCI and other incompressible phases.

To be concrete, we consider the distortion f on an LLL-like flatband. In the monomial basis, the parametrized function is expanded as $h(x) = \sum_{\ell, m} h_{\ell, m} k_1^{m+1} k_2^{\ell+1}$ to generate a superposition of higher angular momentum modes. We choose $h(x) = \epsilon(k_1 \pm ik_2)^2$ to generate the angular momentum-2 mode with opposite chirality. The

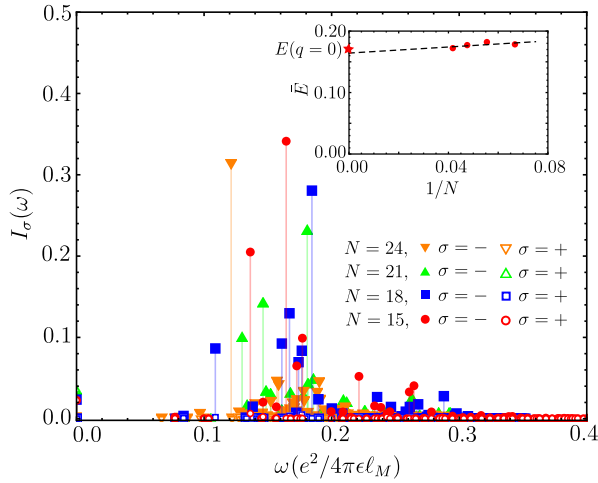


FIG. 3. Spectral weight functions $I_\sigma(\omega)$ for the angular momentum-2 operators with opposite chiralities ($\sigma = +, -$) in FCI, computed by using different numbers of k-points (N), corresponding to different system sizes. The inset is the extrapolation of average energy $\bar{E} = \int \omega I(\omega) d\omega$ at the large system size limit. The red star $E(q=0)$ is the extrapolation of zero momentum magnetoroton energy in the SMA.

Berry connection and quantum metric then transform as $\delta_f A = 0, \delta_f g = \epsilon(\sigma_z \pm i\sigma_x)$. The resulting operator is $\hat{\mathcal{O}}_\pm = \sum_{\mathbf{q}} \mathcal{D}_\pm(\mathbf{q}) V(\mathbf{q}) : \hat{\rho}(-\mathbf{q}) \hat{\rho}(\mathbf{q}) :$, $\mathcal{D}_\pm(\mathbf{q}) = \delta_f g_{\mu\nu} q^\mu q^\nu = (q_1 \pm iq_2)^2$, which has been derived in [45] using anisotropy deformation. In the twisted MoTe₂ system, we further incorporate the C_{3v} lattice symmetry and the translation invariance [51]. The underlying form of $\mathcal{D}_\pm(\mathbf{q})$ are periodic functions in each BZ and behave as $(q_x \pm iq_y)^2$ in the long-wavelength limit in the E representations of C_{3v} [68]. We consider the spectral function $I_\pm(E) = \sum_n |\langle \psi_n | \hat{\mathcal{O}}_\pm | \psi_0 \rangle|^2 \delta(E_n - E)$ of operator $\hat{\mathcal{O}}_\pm$, $|\psi_0\rangle$ is the ground state and $|\psi_n\rangle$ is the eigenstates. To compare the spectral weight of different chiralities, $I_\pm(E)$ is normalized by $\langle \psi_0 | \hat{\mathcal{O}}_-^\dagger \hat{\mathcal{O}}_- | \psi_0 \rangle$.

As shown in Fig. 3, over 90% weight of spectral function resides in the region of $0.10 \sim 0.20e^2/(4\pi\epsilon l_M)$. In the inset of Fig. 3, the extrapolation to the large system size indicates an excitation energy $\bar{E} = \int d\omega \omega I(\omega) \approx 0.1642e^2/(4\pi\epsilon l_M)$, which is close to the long-wavelength magnetoroton energy $E(q=0) \approx 0.165e^2/(4\pi\epsilon l_M)$ derived from the GMP ansatz, suggesting the long-wavelength magnetoroton $\hat{\rho}(\mathbf{q})|\psi_0\rangle, \mathbf{q} \rightarrow 0$ in Fig. 1 can be interpreted as the geometric excitations in FCI. The results unequivocally show that the negative chiral excitations dominate while the positive chiral excitations are negligible, indicating that those excitations are featured with a chiral nature.

By tuning the displacement field or twisted angle, when the low-energy band gets dispersive, FCI becomes less stable and the highly concentrated peaks in the spectral weight functions are broadened (Fig. 4), signaling the reduced stability of geometric excitations. Meanwhile, a

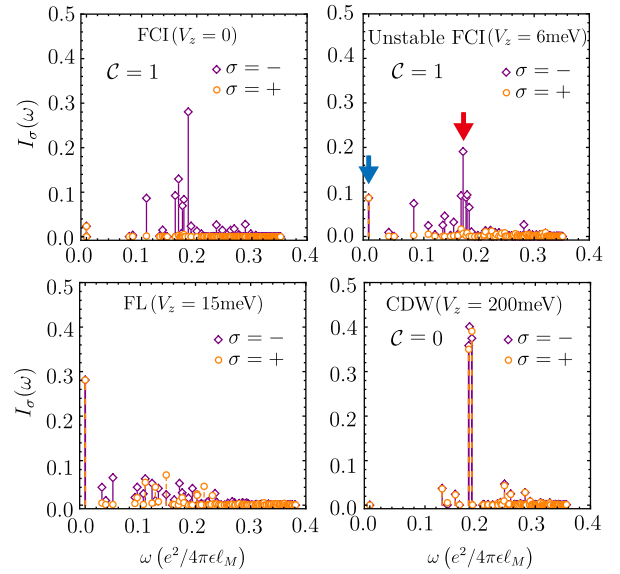


FIG. 4. Spectral weight function of the angular momentum-2 operator for FCI ($V_z = 0$), unstable FCI ($V_z = 6\text{meV}$), FL ($V_z = 15\text{meV}$) and CDW ($V_z = 200\text{meV}$). σ denotes the chirality of the excitations. For ideal FCI, the geometric excitations are chiral and gapped. The gapped chiral excitations (red arrow) are diminished for unstable FCI, and gapless signals with equal chirality (blue arrow) appear. The gapless modes dominate in FL. In CDW, the geometric excitations become gapped and nonchiral.

growing gapless nonchiral signal is observed. The competition of gapless and gapped modes can be considered the new indicators of FCI stability from the perspective of excitations. When the gap closes, the system enters into FL phases, which can still be considered as incompressible fluid in phase space according to Luttinger theorem [69, 70], the gapless signals dominate due to the vanishing renormalized interaction, signaling that the vanishing of geometric excitations in FL.

At the flatband CDW phase, the spectrum exhibits a sharp peak near the many-body gap. Moreover, a prominent feature of the spectrum is that the opposite chiral branches become almost identical, suggesting that the long-wavelength excitations are nonchiral. A possible physical picture is that the electron residing at k point locally experiences the Berry curvature $\Omega_{\mathbf{k}}$ as the effective magnetic field. Electrons that experience magnetic fields in opposite directions contribute to opposite chiralities. For a $\mathcal{C} = 0$ band, the Berry curvature can be somewhere positive and negative, and the numbers of electrons that experience the opposite magnetic field are nearly equal to each other when opposite chiral branches are equivalently involved in the geometric excitations. We verify it by calculating $\bar{B} = \sum_{\mathbf{k}} n_{\mathbf{k}} \Omega_{\mathbf{k}} / N$, where $n_{\mathbf{k}}$ is the charge density at k point. We find that $\bar{B} \sim 10^{-3}$ in the CDW ($V_z = 200\text{meV}$). For comparison, $\bar{B} \sim 1$ in the FCI ($V_z = 0$) [71].

Experiment realization.— To probe the signal of neutral excitations, it is feasible to apply the resonant inelastic light scattering (RILS) in the twisted MoTe₂ or multilayer graphenes. RILS is able to detect the low-lying neutral excitations in FQH liquids [49, 72] and observe the interband excitons in the twisted WSe₂ [73]. It is feasible to identify magnetoroton modes via the recognition of peaks of the density of states at the predicted characteristic scale. It is also likely to find other co-existing excitations, such as magnons [74] in the spin-valley polarized states, or competing excitations which tend to destroy the magnetorotons such as interband excitations due to the prominent band mixing effects [75]. We will leave the study of these possible excitations to future work. To capture the features of excitations in the long-wavelength limit, the circularly polarized resonant inelastic light scattering (CP-RILS) [49] is suggested. CP-RILS can effectively probe the angular momenta of the excitations and thus has the potential to detect the magnetorotons in the long-wavelength limit.

Discussion.— In this work, we study the magnetorotons in the moiré FCIs, using the twisted MoTe₂ as an example. We identify the universal existence of the magnetoroton and predict their characteristic energy and wavelength scale, which is instructive for future experiments. We elucidate the geometric nature of the long-wavelength magnetorotons in FCI and find it can be associated with incompressibility in momentum space. Utilizing the excellent tunability of the moiré system, we extend the discussion to the other incompressible phases, where we find such geometric excitations naturally come from the volume-preserving symmetry in phase space and reduce to position (momentum) subspace in FQH or ideal FCI. The behaviors of geometric excitations relate closely to the band geometry and topology. In a nutshell, the study provides a comprehensive study of the magnetorotons in the moiré FCI, making essential progress in understanding moiré FCI from the perspective of excitations, and evoking further interest in searching for the geometric excitations in other fractionally filled phases.

Acknowledgements.— We thank the stimulating discussion with Lingjie Du, Yiyang Jiang, Steven Simon, Dam Thanh Son, Yuzhu Wang, Zhengzhi Wu, Bo Yang, Kun Yang and Zijian Zhou. This work was supported by the National Key Basic Research and Development Program of China (grant no. 2024YFA1409100), the Basic Science Center Project of NSFC (grant no. 52388201), the National Natural Science Foundation of China (grants no. 12334003, no. 12421004, and no. 12361141826), the National Key Basic Research and Development Program of China (grant no.2023YFA1406400), and the National Science Fund for Distinguished Young Scholars (grant no. 12025405). The calculations were performed at National Supercomputer Center in Tianjin using the Tianhe new generation supercomputer.

* These authors contributed equally to the work.

† chongwang@mail.tsinghua.edu.cn

‡ duanw@tsinghua.edu.cn

§ yongxu@mail.tsinghua.edu.cn;

- [1] J. Cai, E. Anderson, C. Wang, X. Zhang, X. Liu, W. Holtzmann, Y. Zhang, F. Fan, T. Taniguchi, K. Watanabe, Y. Ran, T. Cao, L. Fu, D. Xiao, W. Yao, and X. Xu, Signatures of fractional quantum anomalous hall states in twisted mote2, *Nature* **622**, 63 (2023).
- [2] H. Park, J. Cai, E. Anderson, Y. Zhang, J. Zhu, X. Liu, C. Wang, W. Holtzmann, C. Hu, Z. Liu, T. Taniguchi, K. Watanabe, J.-H. Chu, T. Cao, L. Fu, W. Yao, C.-Z. Chang, D. Cobden, D. Xiao, and X. Xu, Observation of fractionally quantized anomalous hall effect, *Nature* **622**, 74 (2023).
- [3] F. Xu, Z. Sun, T. Jia, C. Liu, C. Xu, C. Li, Y. Gu, K. Watanabe, T. Taniguchi, B. Tong, J. Jia, Z. Shi, S. Jiang, Y. Zhang, X. Liu, and T. Li, Observation of integer and fractional quantum anomalous hall effects in twisted bilayer mote2, *Phys. Rev. X* **13**, 031037 (2023).
- [4] Z. Lu, T. Han, Y. Yao, A. P. Reddy, J. Yang, J. Seo, K. Watanabe, T. Taniguchi, L. Fu, and L. Ju, Fractional quantum anomalous hall effect in multilayer graphene, *Nature* **626**, 759 (2024).
- [5] Y. Xie, A. T. Pierce, J. M. Park, D. E. Parker, E. Khalaf, P. Ledwith, Y. Cao, S. H. Lee, S. Chen, P. R. Forrester, *et al.*, Fractional chern insulators in magic-angle twisted bilayer graphene, *Nature* **600**, 439 (2021).
- [6] K. Kang, B. Shen, Y. Qiu, Y. Zeng, Z. Xia, K. Watanabe, T. Taniguchi, J. Shan, and K. F. Mak, Evidence of the fractional quantum spin hall effect in moiré mote2, *Nature* **628**, 522 (2024).
- [7] Y. Zeng, Z. Xia, K. Kang, J. Zhu, P. Knüppel, C. Vaswani, K. Watanabe, T. Taniguchi, K. F. Mak, and J. Shan, Thermodynamic evidence of fractional chern insulator in moiré mote2, *Nature* **622**, 69 (2023).
- [8] J. Xie, Z. Huo, X. Lu, Z. Feng, Z. Zhang, W. Wang, Q. Yang, K. Watanabe, T. Taniguchi, K. Liu, Z. Song, X. C. Xie, J. Liu, and X. Lu, Even- and odd-denominator fractional quantum anomalous hall effect in graphene moire superlattices (2024), [arXiv:2405.16944](https://arxiv.org/abs/2405.16944).
- [9] C. Nayak, S. H. Simon, A. Stern, M. Freedman, and S. Das Sarma, Non-abelian anyons and topological quantum computation, *Rev. Mod. Phys.* **80**, 1083 (2008).
- [10] A. Y. Kitaev, Fault-tolerant quantum computation by anyons, *Annals of physics* **303**, 2 (2003).
- [11] H. Li, U. Kumar, K. Sun, and S.-Z. Lin, Spontaneous fractional Chern insulators in transition metal dichalcogenide moiré superlattices, *Phys. Rev. Res.* **3**, L032070 (2021).
- [12] T. Devakul, V. Crépel, Y. Zhang, and L. Fu, Magic in twisted transition metal dichalcogenide bilayers, *Nat. Commun.* **12**, 6730 (2021).
- [13] A. Abouelkomsan, Z. Liu, and E. J. Bergholtz, Particle-hole duality, emergent fermi liquids, and fractional chern insulators in moiré flatbands, *Phys. Rev. Lett.* **124**, 106803 (2020).
- [14] C. Repellin and T. Senthil, Chern bands of twisted bilayer graphene: Fractional chern insulators and spin phase transition, *Phys. Rev. Res.* **2**, 023238 (2020).
- [15] P. Wilhelm, T. C. Lang, and A. M. Läuchli, Interplay of

- fractional chern insulator and charge density wave phases in twisted bilayer graphene, *Phys. Rev. B* **103**, 125406 (2021).
- [16] H. Goldman, A. P. Reddy, N. Paul, and L. Fu, Zero-field composite fermi liquid in twisted semiconductor bilayers, *Phys. Rev. Lett.* **131**, 136501 (2023).
- [17] P. J. Ledwith, A. Vishwanath, and D. E. Parker, Vortexability: A unifying criterion for ideal fractional chern insulators, *Phys. Rev. B* **108**, 205144 (2023).
- [18] C. Wang, X.-W. Zhang, X. Liu, Y. He, X. Xu, Y. Ran, T. Cao, and D. Xiao, Fractional chern insulator in twisted bilayer mote_2 , *Phys. Rev. Lett.* **132**, 036501 (2024).
- [19] R. Roy, Band geometry of fractional topological insulators, *Phys. Rev. B* **90**, 165139 (2014).
- [20] N. Regnault and B. A. Bernevig, Fractional chern insulator, *Phys. Rev. X* **1**, 021014 (2011).
- [21] X.-L. Qi, Generic wave-function description of fractional quantum anomalous hall states and fractional topological insulators, *Phys. Rev. Lett.* **107**, 126803 (2011).
- [22] T. S. Jackson, G. Möller, and R. Roy, Geometric stability of topological lattice phases, *Nat. Commun.* **6** (2015).
- [23] S. A. Parameswaran, R. Roy, and S. L. Sondhi, Fractional quantum hall physics in topological flat bands, *Comptes Rendus Physique* **14**, 816–839 (2013).
- [24] J. Wang, J. Cano, A. J. Millis, Z. Liu, and B. Yang, Exact landau level description of geometry and interaction in a flatband, *Phys. Rev. Lett.* **127**, 246403 (2021).
- [25] C. Wang, X. Shen, R. Guo, C. Wang, W. Duan, and Y. Xu, Fractional chern insulators in moiré flat bands with high chern numbers (2024), [arXiv:2408.03305](https://arxiv.org/abs/2408.03305).
- [26] A. P. Reddy, N. Paul, A. Abouelkomsan, and L. Fu, Non-abelian fractionalization in topological minibands, *Phys. Rev. Lett.* **133**, 166503 (2024).
- [27] C.-E. Ahn, W. Lee, K. Yananose, Y. Kim, and G. Y. Cho, Non-abelian fractional quantum anomalous hall states and first landau level physics of the second moiré band of twisted bilayer mote_2 , *Phys. Rev. B* **110**, L161109 (2024).
- [28] H. Lu, B.-B. Chen, H.-Q. Wu, K. Sun, and Z. Y. Meng, Thermodynamic response and neutral excitations in integer and fractional quantum anomalous hall states emerging from correlated flat bands, *Phys. Rev. Lett.* **132** (2024).
- [29] C. Repellin, T. Neupert, Z. Papić, and N. Regnault, Single-mode approximation for fractional chern insulators and the fractional quantum hall effect on the torus, *Phys. Rev. B* **90** (2014).
- [30] X. Hu, D. Xiao, and Y. Ran, Hyperdeterminants and composite fermion states in fractional chern insulators, *Phys. Rev. B* **109**, 245125 (2024).
- [31] S. M. Girvin, A. H. MacDonald, and P. M. Platzman, Magneto-roton theory of collective excitations in the fractional quantum hall effect, *Phys. Rev. B* **33**, 2481 (1986).
- [32] W. Kohn, Cyclotron resonance and de haas-van alphen oscillations of an interacting electron gas, *Phys. Rev.* **123**, 1242 (1961).
- [33] S. Mukherjee and S. S. Mandal, Anomalously low magnetoroton energies of the unconventional fractional quantum hall states of composite fermions, *Phys. Rev. Lett.* **114**, 156802 (2015).
- [34] T. M. R. Wolf, Y.-C. Chao, A. H. MacDonald, and J. J. Su, Intraband collective excitations in fractional chern insulators are dark (2024), [arXiv:2406.10709](https://arxiv.org/abs/2406.10709).
- [35] L. Cavicchi, K. J. A. Reijnders, M. I. Katsnelson, and M. Polini, Optical properties, plasmons, and orbital skyrme textures in twisted tmds (2024), [arXiv:2410.18025](https://arxiv.org/abs/2410.18025).
- [36] A. Gromov and D. T. Son, Bimetric Theory of Fractional Quantum Hall States, *Phys. Rev. X* **7**, 041032 (2017).
- [37] F. D. M. Haldane, E. H. Rezayi, and K. Yang, Graviton chirality and topological order in the half-filled landau level, *Phys. Rev. B* **104** (2021).
- [38] D. T. Son, Is the composite fermion a dirac particle?, *Phys. Rev. X* **5**, 031027 (2015).
- [39] F. D. M. Haldane, Self-duality and long-wavelength behavior of the landau-level guiding-center structure function, and the shear modulus of fractional quantum hall fluids (2011), [arXiv:1112.0990](https://arxiv.org/abs/1112.0990).
- [40] A. G. Abanov and A. Gromov, Electromagnetic and gravitational responses of two-dimensional noninteracting electrons in a background magnetic field, *Phys. Rev. B* **90**, 014435 (2014).
- [41] J. Maciejko, B. Hsu, S. A. Kivelson, Y. Park, and S. L. Sondhi, Field theory of the quantum hall nematic transition, *Phys. Rev. B* **88**, 125137 (2013).
- [42] S.-F. Liou, F. D. M. Haldane, K. Yang, and E. H. Rezayi, Chiral gravitons in fractional quantum hall liquids, *Phys. Rev. Lett.* **123**, 146801 (2019).
- [43] D. X. Nguyen, F. D. M. Haldane, E. H. Rezayi, D. T. Son, and K. Yang, Multiple magnetorotons and spectral sum rules in fractional quantum hall systems, *Phys. Rev. Lett.* **128**, 246402 (2022).
- [44] W. Yuzhu and Y. Bo, Geometric fluctuation of conformal hilbert spaces and multiple graviton modes in fractional quantum hall effect, *Nat. Commun.* **14**, 2317 (2023).
- [45] K. Yang, Acoustic wave absorption as a probe of dynamical geometric response of fractional quantum hall liquids, *Phys. Rev. B* **93**, 161302 (2016).
- [46] Z. Liu, A. Gromov, and Z. Papić, Geometric quench and nonequilibrium dynamics of fractional quantum hall states, *Phys. Rev. B* **98**, 155140 (2018).
- [47] Y.-H. Du, U. Mehta, D. Nguyen, and D. T. Son, Volume-preserving diffeomorphism as nonabelian higher-rank gauge symmetry, *SciPost Physics* **12** (2022).
- [48] A. Pinczuk, B. S. Dennis, L. N. Pfeiffer, and K. West, Observation of collective excitations in the fractional quantum hall effect, *Phys. Rev. Lett.* **70**, 3983 (1993).
- [49] J. Liang, Z. Liu, Z. Yang, Y. Huang, U. Wurstbauer, C. R. Dean, K. W. West, L. N. Pfeiffer, L. Du, and A. Pinczuk, Evidence for chiral graviton modes in fractional quantum hall liquids, *Nature* **628**, 78 (2024).
- [50] M. Kang, A. Pinczuk, B. S. Dennis, L. N. Pfeiffer, and K. W. West, Observation of multiple magnetorotons in the fractional quantum hall effect, *Phys. Rev. Lett.* **86**, 2637 (2001).
- [51] F. Wu, T. Lovorn, E. Tutuc, I. Martin, and A. H. MacDonald, Topological insulators in twisted transition metal dichalcogenide homobilayers, *Phys. Rev. Lett.* **122**, 086402 (2019).
- [52] C. Xu, J. Li, Y. Xu, Z. Bi, and Y. Zhang, Maximally localized wannier functions, interaction models, and fractional quantum anomalous hall effect in twisted bilayer mote_2 , *Proc. Natl. Acad. Sci.* **121**, e2316749121 (2024).
- [53] P. Sharma, Y. Peng, and D. N. Sheng, Topological quantum phase transitions driven by displacement fields in the twisted mote_2 bilayers (2024), [arXiv:2405.08181](https://arxiv.org/abs/2405.08181).
- [54] A. P. Reddy, F. Alsallom, Y. Zhang, T. Devakul, and L. Fu, Fractional quantum anomalous hall states in twisted bilayer mote_2 and wse_2 , *Phys. Rev. B* **108**,

- 085117 (2023).
- [55] X. Shen, C. Wang, R. Guo, Z. Xu, W. Duan, and Y. Xu, Stabilizing fractional chern insulators via exchange interaction in moiré systems (2024), [arXiv:2405.12294](#).
- [56] H. Lu, H.-Q. Wu, B.-B. Chen, and Z. Y. Meng, Vestigial gapless boson density wave emerging between $\nu = 1/2$ fractional chern insulator and finite-momentum supersolid (2024), [arXiv:2408.07111](#).
- [57] J. Yu, J. Herzog-Arbeitman, M. Wang, O. Vafek, B. A. Bernevig, and N. Regnault, Fractional chern insulators versus nonmagnetic states in twisted bilayer mote_2 , *Phys. Rev. B* **109**, 045147 (2024).
- [58] H. Lu, H.-Q. Wu, B.-B. Chen, K. Sun, and Z. Y. Meng, Interaction-driven roton condensation in $\nu = 2/3$ fractional quantum anomalous hall state (2024), [arXiv:2403.03258](#).
- [59] D. Waters, A. Okounkova, R. Su, B. Zhou, J. Yao, K. Watanabe, T. Taniguchi, X. Xu, Y.-H. Zhang, J. Folk, *et al.*, Interplay of electronic crystals with integer and fractional chern insulators in moiré pentalayer graphene, [arXiv preprint arXiv:2408.10133](#) (2024).
- [60] L. Bonsall and A. A. Maradudin, Some static and dynamical properties of a two-dimensional wigner crystal, *Phys. Rev. B* **15**, 1959 (1977).
- [61] T. Tan and T. Devakul, Parent berry curvature and the ideal anomalous hall crystal (2024), [arXiv:2403.04196](#).
- [62] J. Dong, T. Wang, T. Wang, T. Soejima, M. P. Zaletel, A. Vishwanath, and D. E. Parker, Anomalous hall crystals in rhombohedral multilayer graphene i: Interaction-driven chern bands and fractional quantum hall states at zero magnetic field (2024), [arXiv:2311.05568](#).
- [63] Z. Dong, A. S. Patri, and T. Senthil, Theory of quantum anomalous hall phases in pentalayer rhombohedral graphene moiré structures, *Phys. Rev. Lett.* **133**, 206502 (2024).
- [64] H. Lu, H.-Q. Wu, B.-B. Chen, and Z. Y. Meng, From a fractional quantum anomalous hall state to a smectic state with equal hall conductance (2024), [arXiv:2404.06745](#).
- [65] Z. Dong, A. S. Patri, and T. Senthil, Stability of anomalous hall crystals in multilayer rhombohedral graphene, *Phys. Rev. B* **110**, 205130 (2024).
- [66] One can also project the phase space into the momentum space in FQH and consider the LLL in the momentum space.
- [67] In this work, the ideal FCI refers to the FCI hosted in a perfect flatband with topology and geometry identical with LLL.
- [68] In practice, the truncation is set to be $3|\mathbf{G}|$ to ensure the convergence of \mathbf{q} summation. In fact, due to the exponential decay of the form factor, the contribution outside the 1st BZ in summation of \mathbf{q} is strongly suppressed, and hence one can directly apply the $(q_x \pm iq_y)^2$ and set the truncation of the summation up to the 1st BZ.
- [69] J. M. Luttinger, Fermi surface and some simple equilibrium properties of a system of interacting fermions, *Phys. Rev.* **119**, 1153 (1960).
- [70] L. V. Delacrétaz, Y.-H. Du, U. Mehta, and D. T. Son, Nonlinear bosonization of fermi surfaces: The method of coadjoint orbits, *Phys. Rev. Res.* **4**, 033131 (2022).
- [71] We are thankful for Steven Simon for pointing out this.
- [72] C. F. Hirjibehedin, I. Dujovne, A. Pinczuk, B. S. Dennis, L. N. Pfeiffer, and K. W. West, Splitting of long-wavelength modes of the fractional quantum hall liquid at, *Phys. Rev. Lett.* **95** (2005).
- [73] N. Saigal, L. Klebl, H. Lambers, S. Bahmanyar, V. Anić, D. M. Kennes, T. O. Wehling, and U. Wurstbauer, Collective charge excitations between moiré minibands in twisted wse_2 bilayers probed with resonant inelastic light scattering, *Phys. Rev. Lett.* **133**, 046902 (2024).
- [74] T. Wang, T. Devakul, M. P. Zaletel, and L. Fu, Diverse magnetic orders and quantum anomalous hall effect in twisted bilayer mote_2 and wse_2 (2024), [arXiv:2306.02501](#).
- [75] J. Yu, J. Herzog-Arbeitman, M. Wang, O. Vafek, B. A. Bernevig, and N. Regnault, Fractional chern insulators vs. non-magnetic states in twisted bilayer mote_2 (2023), [arXiv:2309.14429](#).
- [76] B. A. Bernevig, Z.-D. Song, N. Regnault, and B. Lian, Twisted bilayer graphene. iii. interacting hamiltonian and exact symmetries, *Phys. Rev. B* **103** (2021).
- [77] B. Andrews, M. Raja, N. Mishra, M. P. Zaletel, and R. Roy, Stability of fractional chern insulators with a non-landau level continuum limit, *Phys. Rev. B* **109**, 245111 (2024).
- [78] M. Claassen, C. H. Lee, R. Thomale, X.-L. Qi, and T. P. Devereaux, Position-momentum duality and fractional quantum hall effect in chern insulators, *Phys. Rev. Lett.* **114** (2015).
- [79] A. Gromov and D. T. Son, Bimetric theory of fractional quantum hall states, *Phys. Rev. X* **7**, 041032 (2017).
- [80] H. Goldman and E. Fradkin, Dirac composite fermions and emergent reflection symmetry about even-denominator filling fractions, *Phys. Rev. B* **98**, 165137 (2018).
- [81] A. C. Balram, Z. Liu, A. Gromov, and Z. Papić, Very-High-Energy Collective States of Partons in Fractional Quantum Hall Liquids, *Phys. Rev. X* **12**, 021008 (2022).
- [82] D. X. Nguyen and D. T. Son, Dirac composite fermion theory of general jain sequences, *Phys. Rev. Res.* **3**, 033217 (2021).
- [83] J. Dong, J. Wang, P. J. Ledwith, A. Vishwanath, and D. E. Parker, Composite fermi liquid at zero magnetic field in twisted mote_2 , *Phys. Rev. Lett.* **131** (2023).
- [84] G. Murthy and R. Shankar, Hamiltonian theories of the fractional quantum hall effect, *Rev. Mod. Phys.* **75**, 1101 (2003).

Supplemental Materials: “Magnetorotons in moiré fractional Chern insulators”

CONTENTS

References	5
I. Continuum model and exact diagonalization	8
II. Numerical details of single mode approximation in FCIs	8
III. Geometric Excitations in Thermodynamic Limit	10
IV. Geometric Excitations in the band system	10
a. Phase space volume-preserving diffeomorphism	11
b. Lowest Landau level in momentum space	12
c. Topological trivial band	13
IV. Trial excitonic wavefunction in moiré FCI	14

I. CONTINUUM MODEL AND EXACT DIAGONALIZATION

The continuum Hamiltonian of the twisted MoTe₂ is

$$\mathcal{H}_\tau(\mathbf{r}) = \begin{pmatrix} -\frac{\hbar^2(\mathbf{k}-\tau\boldsymbol{\kappa}_+)^2}{2m^*} + \Delta_b(\mathbf{r}) + V_z/2 & \Delta_T(\mathbf{r}) \\ \Delta_T^\dagger(\mathbf{r}) & -\frac{\hbar^2(\mathbf{k}-\tau\boldsymbol{\kappa}_-)^2}{2m^*} + \Delta_t(\mathbf{r}) - V_z/2 \end{pmatrix}, \quad (1)$$

where $\tau = \pm 1$ is the spin-valley indices,

$$\begin{aligned} \Delta_{t,b}(\mathbf{r}) &= 2V \sum_{j=1,3,5} \cos(\mathbf{G}_j \cdot \mathbf{r} + \ell\psi), \\ \Delta_T(\mathbf{r}) &= w(1 + e^{-i\tau\mathbf{G}_2 \cdot \mathbf{r}} + e^{-i\tau\mathbf{G}_3 \cdot \mathbf{r}}). \end{aligned} \quad (2)$$

$\Delta_{t,b}(\mathbf{r})$ is the intralayer moiré potential and $\Delta_T(\mathbf{r})$ is the interlayer tunneling terms. $\ell = \pm 1$ is the layer indices. $\mathbf{G}_j, j = 1, \dots, 6$ are the reciprocal lattice vectors. In our numerical calculations, we take the parameters from fitting the first-principles calculation as in: $V = 20.8$ meV, $\psi = 107.7^\circ$ and $w = -23.8$ meV.

From the calculation of the continuum model, the topmost valence band possesses a nearly flat band structure with $\mathcal{C} = 1$. Under the condition of $\epsilon = 5, \theta = 3.89^\circ, d = 30$ nm, the ground state exhibits three-fold ground states at Γ point, serving as the indicator that the system is in the FCI phase. See Fig. 5 for the band structure and ED spectrum.

II. NUMERICAL DETAILS OF SINGLE MODE APPROXIMATION IN FCIS

In this section, we discuss in numerical detail how to construct the GMP wavefunction from the SMA in FCIs. In general, we construct the GMP wavefunction according to

$$|\psi_{\mathbf{q}}\rangle = \hat{\rho}(\mathbf{q})|\psi_0^m\rangle, m = 1, 2, 3 \quad (3)$$

as shown in Fig. 6.

In the $-\frac{2}{3}$ filling, we have three-fold ground degeneracy, and the distribution of the ground states depends on the discretization, or more specifically the generalized Pauli principle. This imposes a possible issue for the ansatz: when the ground state does not reside at the Γ point, which leads to the non-zero overlap between the GMP wavefunction and the ground states, suggesting the ansatz is not effective at those momenta. To avoid this problem, we choose the 3×6 points at most of the calculations, in which the three-fold ground states are all located in the Γ points to ensure

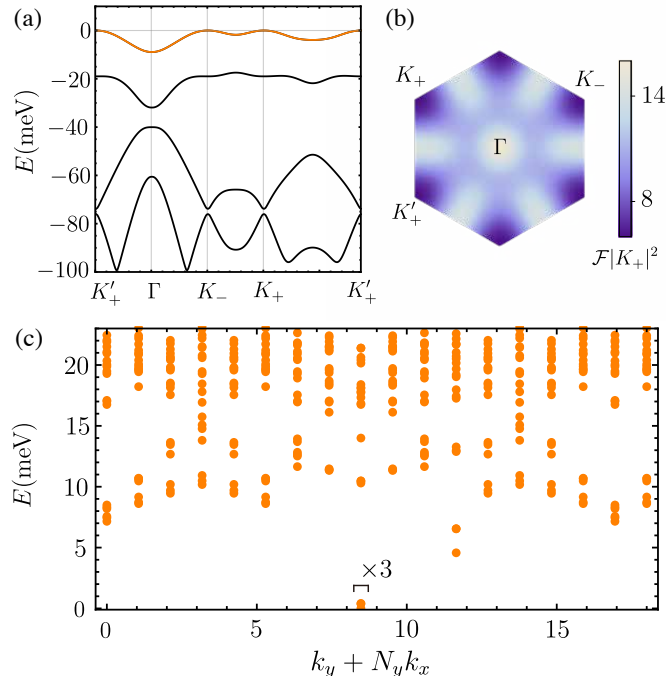


FIG. 5. (a) Band structure of twisted MoTe₂ at $\theta = 3.89^\circ$. The topmost valence band is highlighted in orange. (b) Berry curvature \mathcal{F} of the topmost valence band. (c) Many-body spectrum from the $N = 18$ exact diagonalization in $\epsilon = 5, \theta = 3.89^\circ, d = 30\text{nm}$.

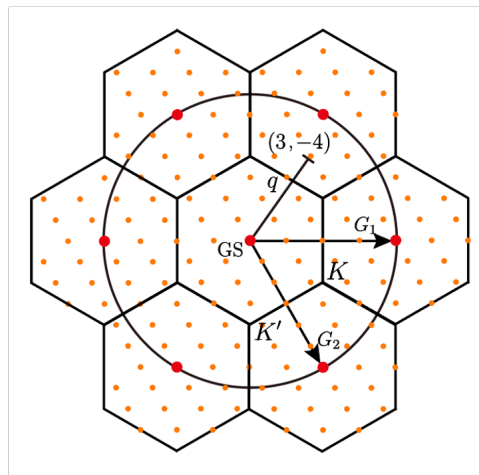


FIG. 6. Schematic representation of the SMA construction in the twisted TMD. The central hexagon region is the 1st BZ and the adjacent hexagons are the 2nd BZs. The orange points are the discretization (e.g. $N_1 = 4, N_2 = 6$) in exact diagonalization calculations. The coordinate $(3, -4)$ represents point $\frac{3}{4}\mathbf{G}_1 - \frac{4}{6}\mathbf{G}_2$. The red points are the Γ points where the ground states reside.

the GMP wavefunctions are orthogonal to the ground states at other momenta. We also calculated $N = 24, 30$ in practice and did not find obvious differences between different clusters.

Another issue is that the single mode approximation is not precise at large \mathbf{q} , hence we restrict ourselves inside the second BZ, say $|\mathbf{q}| < |\mathbf{G}|$.

III. GEOMETRIC EXCITATIONS IN THERMODYNAMIC LIMIT

This section provides information on the energy of angular momentum-2 geometric excitations in the many-body spectrum for various system sizes. The parameters in Sec. I are used. As shown in Fig. 7, we find that for small system sizes the energy of the geometric excitations (the maximum peak of the dynamical spectrum of the operator \hat{O}), highlighted in red, lies inside the continuum excitations region. However, as the increasing of system size, the energy of geometric excitations gets close to the lower bound of the continuum excitations region. For system size 4×6 and 5×6 , the geometric excitations are lying below the continuum excitation region of the many-body spectrum, which suggests in the system the geometric excitations serve as the low-lying excitations compared with the continuum of high energy excitations, and is possible to distinguish from the continuum. It provides evidence that under these conditions, the boundary location of the geometric excitations prevents the diverging of the density of states, henceforth the peaks of geometric excitations may survive in the thermodynamic limit. This suggests the possibility of experimental detection in the thermodynamic limit.

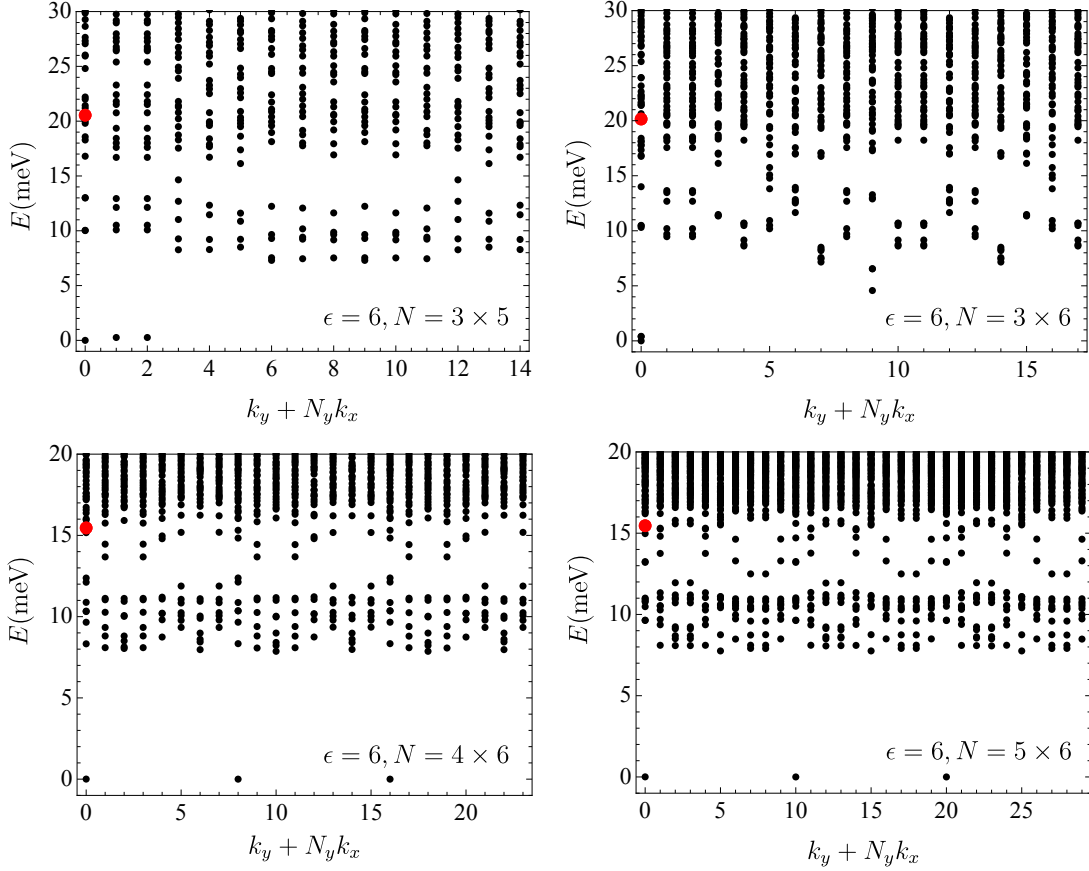


FIG. 7. Position of geometric excitations in the many-body spectrum for $N = 3 \times 5, 3 \times 6, 4 \times 6, 5 \times 6$. The energy of geometric excitations are highlighted in red.

IV. GEOMETRIC EXCITATIONS IN THE BAND SYSTEM

In this section, we try to present the details of geometric excitations in the moiré flatband system and deduce the general form of the operator that is responsible for the system's geometric dynamics. We comes to the conclusion that the geometric excitations in FCI arise due to the incompressibility in the phase space. In particular, we discuss in the context of the $2D$ moiré band system mentioned above.

a. Phase space volume-preserving diffeomorphism

We first give the formal definition of volume-preserving diffeomorphism. Starting from a diffeomorphism in the d dimensional space, we have

$$f : \mathbf{x}_\alpha \rightarrow \mathbf{x}'_\alpha = \mathbf{x}_\alpha + \epsilon v_\alpha(\mathbf{x}), \alpha = 1, \dots, d, \quad (4)$$

\mathbf{x} is the d dimensional coordinates. In the following of considering the transformation of other quantities under the diffeomorphism, we will focus on the *active* diffeomorphism instead of simply doing the coordinate transformation, which is called the *passive* diffeomorphism. The active diffeomorphism means after dragging the coordinates along the manifolds, we perform the coordinate transformation back to the original coordinates and compare the functions at the same point. The active diffeomorphism then naturally relates different geometric quantities in the same coordinates. We consider the Riemannian flat space. Under active diffeomorphism, we write down the transformation of a flat metric

$$\delta'_{\alpha\beta}(\mathbf{x}) = \delta_{\alpha\beta} + \epsilon \partial_\alpha v^\beta(\mathbf{x}) + \epsilon \partial_\beta v^\alpha(\mathbf{x}), \alpha, \beta = 1, \dots, d. \quad (5)$$

The local volume form in the space $\text{Vol}_\delta = \sqrt{\det \delta} dx_1 \wedge dx_2 \wedge \dots \wedge dx_d$ now changes under the active diffeomorphism

$$\text{Vol}_\delta = \sqrt{\det \delta} dx_1 \wedge dx_2 \wedge \dots \wedge dx_d \rightarrow \text{Vol}_{\delta'} = \sqrt{\det \delta'(\mathbf{x})} dx_1 \wedge dx_2 \wedge \dots \wedge dx_d = \sqrt{\det \delta} (1 - \epsilon \partial_\mu v^\mu(\mathbf{x})) dx_1 \wedge dx_2 \wedge \dots \wedge dx_d, \quad (6)$$

By requiring the invariant space volume $\text{Vol}_\delta = \text{Vol}_{\delta'}$, we have $\partial_\mu v^\mu(\mathbf{x}) = 0$. A general solution would be $v^\mu = \epsilon^{\mu\nu} \partial_\nu h(\mathbf{x})$, where h is a differentiated function of \mathbf{x} . The volume perserving diffeomorphism f (VPD) forms a group $\text{SDiff}(\mathbb{R}^d)$. Let us now consider the 4D phase space with $\mathbf{x} = (x_1, x_2, k_1, k_2)$. In the phase space, $x_\alpha, k_\alpha, \alpha = 1, 2$ are conjugated variables to each other $[x_\alpha, p_\beta] = \delta_{\alpha\beta}$. The canonical transformation F that preserves the commutator is

$$F_\alpha : x'_\alpha \rightarrow x_\alpha + \epsilon \nabla_{k_\alpha} h(\mathbf{x}), \quad k'_\alpha \rightarrow k_\alpha - \epsilon \nabla_{x_\alpha} h(\mathbf{x}), \alpha = 1, 2. \quad (7)$$

According to the VPD defined above, the canonical transformation F preserves the phase space volume element $dx_\alpha \wedge dk_\alpha$ invariant, and indicates the incompressibility in phase space.

The algebra of the canonical transformation is generated by $\hat{\mathcal{G}}_h = \epsilon^{ij} \nabla_i h(\mathbf{x}) \cdot \nabla_j, i, j = \mathbf{x}, \mathbf{p}$, and the generator satisfies

$$[\hat{\mathcal{G}}_{h_1}, \hat{\mathcal{G}}_{h_2}] = \hat{\mathcal{G}}_{[h_1, h_2]}, \quad (8)$$

where $[h_1, h_2] = \nabla_{\mathbf{x}} h_1(\mathbf{x}) \cdot \nabla_{\mathbf{p}} h_2(\mathbf{x}) - \nabla_{\mathbf{p}} h_1(\mathbf{x}) \cdot \nabla_{\mathbf{x}} h_2(\mathbf{x})$. It is more convenient to phrase the algebra on a suitable basis. This can be achieved by choosing the monomial basis $h(\mathbf{x}) = -\sum_{\ell, m} h_{n, m}^{j, k} x_1^{j+1} x_2^{k+1} k_1^{n+1} k_2^{m+1}$, and the generator takes the form $\hat{\mathcal{G}}_h = \sum_{j, k, m, n} h_{n, m}^{j, k} \hat{\mathcal{L}}_{n, m}^{j, k}$, where the $\hat{\mathcal{L}}_{n, m}^{j, k}$ obey the algebra

$$\begin{aligned} [\hat{\mathcal{L}}_{n_1, m_1}^{j_1, k_1}, \hat{\mathcal{L}}_{n_2, m_2}^{j_2, k_2}] &= ((j_2 + 1)(n_1 + 1) - (j_1 + 1)(n_2 + 1)) \hat{\mathcal{L}}_{n_1 + n_2, m_1 + m_2 + 1}^{j_1 + j_2, k_1 + k_2 + 1} \\ &\quad + ((k_2 + 1)(m_1 + 1) - (k_1 + 1)(m_2 + 1)) \hat{\mathcal{L}}_{n_1 + n_2 + 1, m_1 + m_2}^{j_1 + j_2 + 1, k_1 + k_2}. \end{aligned} \quad (9)$$

In general, the geometric excitations generated by $\hat{\mathcal{L}}_{n, m}^{j, k} |0\rangle$ can be considered as the distortion mode of the space-momentum mixed space. It is direct to check the algebra contains 2 sets of commuting subalgebra $\text{sdiff}(\mathbb{R}^2)$, or 2D classical w_∞ algebra formed by $\hat{\mathcal{L}}_{-1, m}^{-1, k}$ and $\hat{\mathcal{L}}_{n, -1}^{j, -1}$, within each sector the higher spin mode can be defined as the ‘‘phase space higher spin mode’’.

$$[\hat{\mathcal{L}}_m^k, \hat{\mathcal{L}}_n^j] = ((m + 1)(j + 1) - (n + 1)(k + 1)) \hat{\mathcal{L}}_{m+n}^{k+j}, \quad \hat{\mathcal{L}}_m^k = \hat{\mathcal{L}}_{m, -1}^{k, -1}. \quad (10)$$

The band projection in LLL relates $x_1 \rightarrow k_2, x_2 \rightarrow k_1$, thus unifying 2 sets of 2D w_∞ algebra and projecting the 2D phase space to the momentum or real subspace. The corresponding phase space geometric excitations then become the real space or momentum space geometric excitations.

In general, the interaction does not commute with the generators \mathcal{L} , henceforth the VPD modes are likely to consume energy and acquire an energy gap. We will now consider the change of action or Hamiltonian under VPD by taking account into the interaction. For simplicity, in the following discussion, we assume the interaction $V(\mathbf{q})$ is isotropic, which amounts to neglecting the anisotropy in the dielectric constant and projected to the single valence band. The projected interaction term dominating the kinetic term is

$$V = \frac{1}{2A} \sum_{\mathbf{q}} V(\mathbf{q}) \hat{\rho}(\mathbf{q}) \hat{\rho}(-\mathbf{q}) = \frac{1}{2A} \sum_{\mathbf{k}, \mathbf{k}', \mathbf{q}} V(\mathbf{q}) \Lambda_{\mathbf{k}, \mathbf{q}} \Lambda_{\mathbf{k}', -\mathbf{q}} \hat{c}_{\mathbf{k}+\mathbf{q}}^\dagger \hat{c}_{\mathbf{k}'-\mathbf{q}}^\dagger \hat{c}_{\mathbf{k}'} \hat{c}_{\mathbf{k}}, \quad (11)$$

$\Lambda_{\mathbf{k}, \mathbf{q}}$ is the form factor $\langle u_{\mathbf{k}+\mathbf{q}} | u_{\mathbf{k}} \rangle$, which is not gauge invariant and need gauge fixing [76, 77]. Let's now assume the form factor is fast decay versus \mathbf{q} , so that we can set the truncation of \mathbf{q} small enough to validate the small \mathbf{q} expansion. By directly expanding, we have

$$\begin{aligned} \Lambda_{\mathbf{k}, \mathbf{q}} &= 1 - i \langle u_{\mathbf{k}} | \partial_\mu u_{\mathbf{k}} \rangle dq^\mu + \frac{1}{2} \langle u_{\mathbf{k}} | \partial_\mu \partial_\nu u_{\mathbf{k}} \rangle dq^\mu dq^\nu + \mathcal{O}(q^3) \\ &= 1 - i A_\mu(\mathbf{k}) dq^\mu + \frac{1}{2} A_\mu(\mathbf{k}) A_\nu(\mathbf{k}) dq^\mu dq^\nu - \frac{1}{2} g_{\mu\nu}(\mathbf{k}) dq^\mu dq^\nu + \frac{1}{4} (\partial_\nu A_\mu(\mathbf{k}) + \partial_\mu A_\nu(\mathbf{k})) dq^\mu dq^\nu + \mathcal{O}(q^3). \end{aligned} \quad (12)$$

where $A_\mu(\mathbf{k})$ is the Berry connection and $g_{\mu\nu}(\mathbf{k})$ is the Fubini-Study metric. Formally, in an isolated general Bloch band, the geometry of the Bloch state is characterized by the map $P : \text{BZ}^2 \rightarrow \mathbb{C}P^{n-1}$, where BZ^2 is the two-dimensional Brillouin zone and $\mathbb{C}P^{n-1}$ is the $n-1$ dimensional complex projective space characterized by $n-1$ parameters. It is then natural to consider the Fubini-Study metric on the Brillouin zone as the pullback of the standard $\mathbb{C}P^{n-1}$ metric and Berry curvature $\Omega(\mathbf{k})$ as the pullback of the symplectic 2-form in $\mathbb{C}P^{n-1}$. Under the distortion f , the gauge field and the quantum metric in momentum space are then transformed as:

$$\delta_f A_\alpha(\mathbf{k}) = \epsilon(v^\mu \partial_\mu A_\alpha(\mathbf{k}) + A^\mu \partial_\mu v_\alpha(\mathbf{k})), \quad (13)$$

$$\delta_f g_{\alpha\beta}(\mathbf{k}) = \epsilon(v^\sigma \partial_\sigma g_{\alpha\beta}(\mathbf{k}) + g_{\mu\beta} \partial_\alpha v^\mu(\mathbf{k}) + g_{\mu\alpha} \partial_\beta v^\mu(\mathbf{k})). \quad (14)$$

The change of the Hamiltonian under the VPD f , which is the operator $\hat{O} = \delta_f H(A, g)$ in the main context, measures the energy and the dynamical property of geometric excitations.

$$\hat{O}(\mathbf{k}) = \frac{\delta V(A, g)}{\delta A} \delta_f A(\mathbf{k}) + \frac{\delta V(A, g)}{\delta g} \delta_f g(\mathbf{k}). \quad (15)$$

We will focus on several simple cases to derive the explicit form of the operator.

b. Lowest Landau level in momentum space

As a warmup, we first consider the lowest Landau level with the magnetic field $\nabla \times A = -B \cdot \hat{z}$. In this case, the phase and distance factors can be analytically derived by introducing the guiding center \mathbf{R} and Landau orbit $\bar{\mathbf{R}}$

$$\mathbf{R} = \mathbf{r} + \ell_B^2 \boldsymbol{\pi} \times \hat{z} = \mathbf{r} - \bar{\mathbf{R}} \quad (16)$$

$\boldsymbol{\pi} = \mathbf{p} + e\mathbf{A}$ is the momentum that commutes with \mathbf{R} . The Hamiltonian can be written into

$$H = \frac{\boldsymbol{\pi}^2}{2m} = \omega_c (a^\dagger a + \frac{1}{2}), \quad a = \frac{1}{\ell_B \sqrt{2}} (\bar{R}_y - i\bar{R}_x) \quad (17)$$

The magnetic translation operator formed by the guiding center $t(\mathbf{r}) = \exp(i\mathbf{r} \cdot \frac{1}{\ell_B^2} (\hat{z} \times \mathbf{R}))$ satisfies the magnetic translational algebra

$$t(\mathbf{r}_1) t(\mathbf{r}_2) = \exp(i(\mathbf{r}_1 \times \mathbf{r}_2) \cdot \hat{z} / \ell_B^2) t(\mathbf{r}_2) t(\mathbf{r}_1) \quad (18)$$

the magnetic algebra effectively defines a reduced magnetic lattice with unit cell spanned by $\mathbf{a}_1, \mathbf{a}_2$ that encloses $2\pi\ell_B^2$ area penetrated by a flux quanta. Notice the commutator of Landau orbits and guiding center satisfy

$$[R_i, R_j] = -i\epsilon_{ij} \ell_B^2, \quad [\bar{R}_i, \bar{R}_j] = i\epsilon_{ij} \ell_B^2, \quad [R_i, \bar{R}_j] = 0 \quad (19)$$

Since the Hamiltonian only depends on Landau orbits, the eigenvalues can be classified into the Landau levels $E_n = \omega_c(n + \frac{1}{2})$, since the Landau orbits are commute with guiding centers, we can further label the states inside a

Landau level by calculating the eigenvalues of the magnetic translational operators, hence in general a state can be expressed into $|n, \mathbf{k}\rangle$, where n is the n th Landau level and \mathbf{k} is the momentum in the reduced magnetic BZ. Any state with momentum \mathbf{k} inside the reduced magnetic BZ can be generated by applying a boost on a zero-momentum state

$$|n, \mathbf{k}\rangle = \exp(i\mathbf{k} \cdot \mathbf{R})|n, \mathbf{0}\rangle \quad (20)$$

The formfactor of the LLL then goes to

$$\begin{aligned} \Lambda_{\mathbf{k}, \mathbf{q}} &= \langle u_{\mathbf{k}+\mathbf{q}} | u_{\mathbf{k}} \rangle = \langle 0, \mathbf{k} + \mathbf{q} | \exp(i\mathbf{q} \cdot \mathbf{r}) | 0, \mathbf{k} \rangle = \langle 0, \mathbf{k} + \mathbf{q} | \exp(i\mathbf{q} \cdot (\mathbf{R} + \bar{\mathbf{R}})) | 0, \mathbf{k} \rangle \\ &= \langle 0 | \exp(i\bar{\mathbf{R}}) | 0 \rangle \langle \mathbf{k} + \mathbf{q} | \exp(i\mathbf{q} \cdot \mathbf{R}) | \mathbf{k} \rangle = \exp\left[\frac{\ell_B^2}{4}(2i\mathbf{k} \times \mathbf{q} - |\mathbf{q}|^2)\right] \end{aligned} \quad (21)$$

where we have use BHC formula and Eq.(19) when calculating $\langle \mathbf{k} + \mathbf{q} | \exp(i\mathbf{q} \cdot \mathbf{R}) | \mathbf{k} \rangle$

$$\begin{aligned} \langle \mathbf{k} + \mathbf{q} | \exp(i\mathbf{q} \cdot \mathbf{R}) | \mathbf{k} \rangle &= \langle 0 | \exp(-i(\mathbf{q} + \mathbf{k}) \cdot \mathbf{R}) \exp(i\mathbf{q} \cdot \mathbf{R}) \exp(i\mathbf{k} \cdot \mathbf{R}) | 0 \rangle \\ &= \langle 0 | \exp(-i(\mathbf{q} + \mathbf{k}) \cdot \mathbf{R}) \exp(i(\mathbf{q} + \mathbf{k}) \cdot \mathbf{R}) \exp(i\frac{1}{2}\ell_B^2 \epsilon_{ij} q_i k_j) | 0 \rangle \\ &= \exp\left(i\frac{\ell_B^2}{2} \mathbf{k} \times \mathbf{q}\right) \end{aligned} \quad (22)$$

As we have demonstrated above, the formfactor consists of a phase factor under the gauge $A = (-k_2, k_1)\frac{B}{2}$ and a distance factor with quantum metric $g = \frac{1}{2B}\mathbb{I}$. According to the condition of VPD, we choose $h(\mathbf{x}) = k_x k_y$ and the corresponding VPD f is generated to be $f : k_1 \rightarrow k_1 + \epsilon k_1, k_2 \rightarrow k_2 - \epsilon k_2$ as the infinitesimal version of VPD $(k_1, k_2) \rightarrow (ak_1, k_2/a)$. Using Eq.(14), the quantum metric transforms into $g \rightarrow g' = \frac{1}{2B}(\mathbb{I} + \epsilon\sigma_z), A \rightarrow A' = A$ under VPD. The invariant of Berry connection ensures the AB phase factor $\exp(i \int Adq) = \exp(i\frac{1}{2}\mathbf{k} \times \mathbf{q})$ is invariant under VPD.

Under the deformation, the form factor transforms as

$$\Lambda_{\mathbf{k}, \mathbf{q}} \rightarrow \Lambda'_{\mathbf{k}, \mathbf{q}} = \exp\left[\frac{\ell_B^2}{4}(2i\mathbf{k} \times \mathbf{q} - ((1 + \epsilon)q_1^2 + q_2^2(1 - \epsilon)))\right] \approx \Lambda_{\mathbf{k}, \mathbf{q}} - \epsilon\frac{\ell_B^2}{4}(q_1^2 - q_2^2)\Lambda_{\mathbf{k}, \mathbf{q}} \quad (23)$$

inserting into Eq.(11), we have the form of operator that coupled to geometric excitations

$$\hat{\mathcal{O}} = \delta_f V(A, g) \approx \frac{1}{2A} \sum_{\mathbf{q}} \frac{\ell_B^2}{2} (q_2^2 - q_1^2) V(\mathbf{q}) \hat{\rho}(\mathbf{q}) \hat{\rho}(-\mathbf{q}) \quad (24)$$

the operator can be recast into a more general form

$$\hat{\mathcal{O}} = \frac{1}{2A} \sum_{\mathbf{q}} V(\mathbf{q}) (\sigma_z \mathbf{q}) \mathbf{q}^T \hat{\rho}(\mathbf{q}) \hat{\rho}(-\mathbf{q}) \quad (25)$$

The result is applicable to a general gauge that interpolates between the Landau gauge and the symmetric gauge.

c. Topological trivial band

We now consider the Chern band with $\mathcal{C} = 0$ which mimics the topological trivial flatband that supports CDW in the main context. To facilitate the gauge fixing, we set $\Omega_{\mathbf{k}} = 0$. The triviality of $\Omega_{\mathbf{k}}$ allows us to erase the gauge field using the gauge transformation $A'_{\mathbf{k}} \rightarrow A_{\mathbf{k}} - \nabla\phi_{\mathbf{k}} = 0$. Since $\langle u_{\mathbf{k}} | \partial_{\mu} u_{\mathbf{k}} \rangle = 0$, we have $\langle u_{\mathbf{k}} | \partial_{\mu} \partial_{\nu} u_{\mathbf{k}} \rangle + \langle \partial_{\mu} u_{\mathbf{k}} | \partial_{\nu} u_{\mathbf{k}} \rangle = 0$, and henceforth $\text{Im}\langle u_{\mathbf{k}} | \partial_{\mu} \partial_{\nu} u_{\mathbf{k}} \rangle = -\text{Im}\langle \partial_{\mu} u_{\mathbf{k}} | \partial_{\nu} u_{\mathbf{k}} \rangle$. By using the fact that $\langle \partial_{\mu} u_{\mathbf{k}} | \partial_{\nu} u_{\mathbf{k}} \rangle$ is Hermitian, the imaginary part of it is anti-symmetric. Finally, we conclude that $\text{Im}\langle u_{\mathbf{k}} | \partial_{\mu} \partial_{\nu} u_{\mathbf{k}} \rangle$ is also anti-symmetric and do not contribute to the expansion in Eq.(12). The long-wavelength expansion of the formfactor now reduces to

$$\Lambda_{\mathbf{k}, \mathbf{q}} \approx 1 + \frac{1}{2} \text{Re}\langle u_{\mathbf{k}} | \partial_{\mu} \partial_{\nu} u_{\mathbf{k}} \rangle dq^{\mu} dq^{\nu} + \dots = 1 - \frac{1}{2} g_{\mu\nu}(\mathbf{k}) dq^{\mu} dq^{\nu} + \dots, \quad (26)$$

We pick up a canonical transformation generated by $h(\mathbf{x}) = x_1 k_1 - x_2 k_2$ in the phase space to generate the phase space angular momentum-2 mode.

$$k'_1 \rightarrow k_1 + \epsilon \nabla_{x_1} (x_1 k_1 - x_2 k_2), k'_2 \rightarrow k_2 + \epsilon \nabla_{x_2} (x_1 k_1 - x_2 k_2), \quad (27)$$

Explicitly in coordinates, the change of quantum metric is

$$\delta_f g_{11}(\mathbf{k}) = \epsilon(k_1 \partial_1 g_{11} - k_2 \partial_2 g_{11} + 2g_{11})(\mathbf{k}), \quad \delta_f g_{22}(\mathbf{k}) = \epsilon(k_1 \partial_1 g_{22} - k_2 \partial_2 g_{22} - 2g_{22})(\mathbf{k}), \quad (28)$$

$$\delta_f g_{12}(\mathbf{k}) = \delta_f g_{21}(\mathbf{k}) = \epsilon(k_1 \partial_1 g_{12} - k_2 \partial_2 g_{12})(\mathbf{k}). \quad (29)$$

the formfactor under VPD is then

$$\Lambda_{\mathbf{k},\mathbf{q}} \rightarrow \Lambda'_{\mathbf{k},\mathbf{q}} \approx 1 - \frac{1}{2}g'(\mathbf{k})\mathbf{q}\mathbf{q} \approx 1 - \frac{1}{2}g(\mathbf{k})\mathbf{q}\mathbf{q} - \epsilon \left(g(\mathbf{k})(\sigma_z \mathbf{q})(\mathbf{q}) + \frac{1}{2}(\sigma_z \mathbf{k} \cdot \nabla)g(\mathbf{k})\mathbf{q}\mathbf{q} \right). \quad (30)$$

the above expression in general involves metric derivatives, which can not be ignored when the band is strongly dispersive, which might indicate the excitations become unstable away from the flatband limit. This also suggests that when the band gets dispersive, the fluctuation of geometry cannot be ignored and the higher spin mode can be interpreted to live in a ‘‘curved space’’. We drop it under our assumption and leave it for future study. We find that Eq.(30) actually indicates the coupling between the quantum metric g and the flat external auxiliary metric (which has been considered as a band mass tensor in [45]) $\eta = \mathbb{I}$

$$\Lambda'_{\mathbf{k},\mathbf{q}} \approx 1 - \frac{1}{2}g(\mathbf{k})(\eta\mathbf{q})(\mathbf{q}) \quad (31)$$

by deforming the auxiliary flat metric and fixing the quantum metric, we are able to derive the same operator. The deformation of η instead of g actually amounts to the coordinate transformation and is a *passive* perspective to the VPD. This indicates the general form of coupling between quantum metric and external metric $g\eta$. A similar form of coupling has also been revealed in [78] by introducing a quadratic confining potential and bimetric gravity theory [79] which appears in the potential term that leads to the spontaneous symmetry breaking in the isotropic phase.

The operator can be easily found under VPD

$$\hat{O} = \delta_f V(A, g) = \frac{1}{2A} \sum_{\mathbf{q}, \mathbf{k}, \mathbf{k}'} V(\mathbf{q}) \left[(\sigma_z \mathbf{q}) \frac{g(\mathbf{k}) + g(\mathbf{k}')}{2} \mathbf{q}^T \right] \Lambda_{\mathbf{k},\mathbf{q}} \Lambda_{\mathbf{k}',-\mathbf{q}} \hat{c}_{\mathbf{k}+\mathbf{q}}^\dagger \hat{c}_{\mathbf{k}'-\mathbf{q}}^\dagger \hat{c}_{\mathbf{k}'} \hat{c}_{\mathbf{k}} \quad (32)$$

which is the operator responsible for the geometric dynamics of a topological trivial band. Here $\mathbf{q} = (q_x, q_y)$.

IV. TRIAL EXCITONIC WAVEFUNCTION IN MOIRÉ FCI

This section postulates the trial many-body wavefunctions of intraband neutral excitations in twisted MoTe₂. The following discussion is based on the projection on the topmost valence band. Several obstacles exist to constructing the wavefunctions and the corresponding field theory. First of all, the electron is now living in the zero field conditions, or equivalently the flux-attaching process can not be directly applied. Secondly, in the case that the electron is living in the moiré lattice, it is essential for the wavefunction to accommodate the moiré potential and should be compatible with the crystalline symmetry.

Our phenomenological approach is motivated by the parton construction [80–82], where the physical electron c can be decomposed into a bosonic parton χ with charge q_1 and a fermionic parton ϕ [83] with charge $q_2 = 1 - q_1$

$$c = \chi \cdot \phi \quad (33)$$

The $U(1)$ symmetry of the composite form requires the introduction of the auxiliary gauge field a . This gluing gauge field assigns the +1 charge to the bosonic partons and -1 charge to the fermionic partons. The theory in terms of new degrees of freedom is then decomposed into

$$\mathcal{L} = \mathcal{L}_{\text{bosonic}}(\chi, q_1 A + a) + \mathcal{L}_{\text{fermionic}}(\phi, q_2 A - a) \quad (34)$$

Reorganizing the gauge field that interacts with bosonic and fermionic partons to be

$$\alpha_\chi = q_1 A + a, \quad \alpha_\phi = q_2 A - a \quad (35)$$

ϕ parton now is feeling the flux from α_ϕ , $d\alpha_\phi = d(q_2 A - a) = -da$ in the zero external flux case, this means that the existence of the auxiliary gauge field compensates for the zero-flux of the external field. We first condense the

bosonic parton to the superfluid phase that higgs α_χ and then focus on the field theory of the fermionic parton, which is exactly the field theory that resembles the FQH case.

Coincidentally, such a decomposed picture can be visualized in the factorized form of the single particle wavefunction in the ideal $\mathcal{C} = 1$ Chern band in the twisted MoTe₂

$$\psi_{\mathbf{k}\ell}(\mathbf{r}) = \phi_{\mathbf{k}}(\mathbf{r})\zeta_\ell(\mathbf{r}) = f(z)e^{-K(\mathbf{r})}\zeta_\ell(\mathbf{r}) \quad (36)$$

$\ell = \pm 1$ is the layer indices. $\zeta(r)$ is k -independent and encodes the information of the orbital and layer basis. $\phi_k(r)$ describes a fermion residing in the inhomogeneous periodic magnetic field. The single particle wavefunctions indicate that the many-body wave function has the form of

$$\Psi(\{\mathbf{r}_i\}) = \Psi_\phi \Psi_\chi = \Phi(\mathbf{r}_i) \prod_i \zeta_{\ell_i}(\mathbf{r}_i) \quad (37)$$

where Ψ_ϕ is the wavefunctions of the flux-feeling particles. The many-body excitonic function at $\frac{1}{3}$ filling $\Psi_{\nu=\frac{1}{3}}^{\text{exc}}$, in the same manner, is established to be

$$\Psi_{\nu=\frac{1}{3}}^{\text{exc}}(\{\mathbf{r}_i\}) = \Phi_{\nu=\frac{1}{3}}^{\text{exc}}(\mathbf{r}_i) \prod_i \zeta_{\ell_i}(\mathbf{r}_i). \quad (38)$$

where $\Phi_{\nu=\frac{1}{3}}^{\text{exc}}$ is the many-body excitonic wavefunction of the fermionic parton.

Here the excited wavefunction of ϕ -parton $\Phi_{\phi,\nu=1/3}^{\text{exc}}(\{z_i\})$ can be extracted from our SMA ansatz $|\psi_{\text{ex},\mathbf{q}}\rangle = \bar{\rho}_e(\mathbf{q})|\psi_0\rangle$, with the help of the connection between the LLL single-body electronic density operator and the CF density operators. Basically, we can follow the projective construction of composite-fermion states to enlarge the electronic Hilbert space by tensor product with the vortex Hilbert space [30, 84]. And the physical electronic states must satisfy the constraint

$$|\psi_e\rangle \otimes |\psi_v\rangle = \mathcal{P}_v |\psi_{\text{CF}}\rangle, \quad (39)$$

where $\mathcal{P}_v \equiv |\psi_v\rangle\langle\psi_v|$ is the many-body projector of vortex states (as some gauge degree of freedom), which can also be appreciated as LLL projection \mathcal{P}_{LLL} when feeding into Jain's prescription. Generally, however, the electronic many-body wavefunction satisfying Eq.(39) is shown to take the form of *hyperdeterminants* of some tensors [30]. For the $\nu = 1/3$ states here, the vortex states should be bosonic with filling $\nu = 1/2$, and thus it is natural to take a choice of $\nu = 1/2$ bosonic Laughlin states, and the electronic wavefunction reads

$$\Phi_{\nu=1/3}(\{z_{e,i}\}) = \int \mathcal{D}\omega_{v,j} \mathcal{D}\zeta_{\text{CF},k} \psi_{\nu=1/2,v}^{\text{Laughlin}}(\{\omega_{v,j}\})^* \psi_{\text{CF}}(\{\zeta_{\text{CF},k}\}) \langle z_{e,i}, \omega_{v,j} | \zeta_{\text{CF},k} \rangle \quad (40)$$

for the coherent basis of electrons and vortex $\{z_{e,i}\}$ and $\{\omega_{v,j}\}$, and the position basis (delta function) of CFs $\{\zeta_{\text{CF},k}\}$. Here i, j, k are particle index and $\int \mathcal{D}z_\alpha \equiv \int \prod_i \frac{dz_{\alpha,i}}{2\pi\ell_\alpha^2}$ represents the coherent state integration. The fusion coefficients $\langle z_{e,i}, \omega_{v,j} | \zeta_{\text{CF},k} \rangle$ can be evaluated with the help of magnetic translation algebra [30]

$$\langle z_{e,i}, \omega_{v,j} | \zeta_{\text{CF},k} \rangle = \sqrt{\frac{1+c}{1-c}} e^{-\frac{1}{4\ell_v^2}\bar{\omega}\omega + \frac{1}{2\ell_v^2}\bar{\omega}(-\frac{z}{c} + \frac{1+1}{c}\zeta)} e^{-\frac{1}{4\ell_{\text{CF}}^2}\frac{1-c}{1+c}\bar{\zeta}\zeta + \frac{1}{2\ell_{\text{CF}}^2}\frac{\bar{\zeta}z}{1-c}} e^{-\frac{\bar{z}z}{4\ell_e^2}}.$$

Following Murthy-Shankar's composite-fermion substitution [84]

$$\mathcal{R}_e = \mathcal{R} + c\eta, \quad \mathcal{R}_v = \mathcal{R} - \eta/c, \quad (41)$$

the action of the projected electronic density operator $\bar{\rho}_e(\mathbf{q})$ on the ground state then can be lifted to the action within the CF Hilbert space (up to some phases). After fixing the gauge to be consistent with the expectation in the continuum limit, where bare guiding-center coordinates and cyclotron coordinates are all well-defined as Eq.(41), we can lift the action of LLL electronic density operator to CF Hilbert space as

$$\rho_e(\mathbf{q}) = \rho_{\mathcal{R}}(\mathbf{q})\rho_\eta(-c\mathbf{q}), \quad (42)$$

where $\rho_{\mathcal{R}}(\mathbf{q}) = e^{i\mathbf{q}\cdot\mathcal{R}}$ and $\rho_\eta(\mathbf{q}) = e^{-i\mathbf{q}\cdot\eta}$ are the density operator of the CF guiding-center/cyclotron degrees of freedom. Consequently, the excited electronic wavefunction following the SMA approximation can still be obtained

following the projective construction Eq.(39), so will be in a similar form as Eq.(40), but with the new CF wavefunction, i.e., the excited CF wavefunction deviated from the original one due to the lifted action

$$\psi_{\text{CF},\mathbf{q}}(\{\zeta_{\text{CF},k}\}) \equiv \langle \zeta_{\text{CF},k} | \rho_{\mathcal{R}}(\mathbf{q}) \rho_{\boldsymbol{\eta}}(-c\mathbf{q}) | \psi_{\text{CF}} \rangle. \quad (43)$$

To extract the physical essence of this excited CF wavefunction, one just need to remind that \mathcal{R} controls the motion within the CF Landau level, while $\boldsymbol{\eta}$ controls the motion within the $\boldsymbol{\eta}$ -plane constructed in Ref. [30], after the exact mapping from the Landau level indices to a fictitious plane with a different sample size controlled by the fillings hosting a LLL. As a result, any shifts of coherent states within the $\boldsymbol{\eta}$ -plane due to $\rho_{\boldsymbol{\eta}}(\mathbf{q})$ will corresponds to a CF LL index change, so Eq.(43) does represent some superposition of the CF particle-hole excitations, matching the CF understanding of magnetoroton excitations. The discrepancy of SMA to the exact computatoin of magnetoroton excitations will be on the envelope function of CF particle-hole pairs (which is ansatzed here).